International Journal of Fluid Machinery and Systems
Vol. 8, No. 2, April-June 2015

DOI: http://dx.doi.org/10.5293/IJFMS.2015.8.2.084
ISSN (Online): 1882-9554

Original Paper (Invited)

Accelerating CFD-DEM simulation of dilute pneumatic conveying with bends

Jun Du, Guoming Hu, Ziqiang Fang and Wenjie Gui

School of Power and Mechanical Engineering, Wuhan University
Wuhan 430072, China, dujun@whu.edu.cn

Abstract

The computational cost is expensive for CFD-DEM simulation, a larger time step and a simplified CFD-DEM model can be used to accelerate the simulation. The relationship between stiffness and overlap in non-linear Hertzian model is examined, and a reasonable time step is determined by a new single particle test. The simplified model is used to simulate dilute pneumatic conveying with different types of bends, and its applicability is verified by compared with the traditional model. They are good agreement in horizontal-vertical case and vertical-horizontal case, and show a significant differences in horizontal-horizontal case. But the key features of particle rope formed in different types of bends can be obtained by both models.

Keywords: CFD-DEM, dilute pneumatic conveying, time step.

1. Introduction

In recent decades, CFD-DEM proposed by Tsuji *et al.* [1] has been one of the most important numerical methods to research gas-solid flow. In CFD-DEM, the discrete particle phase was obtained by Discrete Element Method (DEM), and the flow of continuum gas phase was determined by Computational Fluid Dynamics (CFD). CFD has been widely accepted in engineering application as its capability to implement complex geometry simulation. Especially with the development of the commercial CFD software package, it continued to expand the scope of application and offered new ways to solve practical engineering problems. DEM was proposed by Cundall and Strack in 1979, which was effective to study particle flow as it accounts for particle-particle and particle-wall interactions. Zhu *et al.* [2,3] reviewed the theoretical developments and major applications and findings of CFD-DEM.

Although the computational power increased rapidly over recent years, the computational cost is still expensive as amounts of calculation of the particle-particle and particle-wall interactions by DEM. There are several approaches that have been used to reduce the computational load of DEM as mentioned by Malone and Xu [4], including the use of more advanced contact detection algorithms, parallel computing techniques, novel numerical time integration schemes, simple contact models, and a larger reasonable time step. Theoretically, all of the approaches can be used to speed up CFD-DEM simulation, but a larger time step seems like a simple one. Meanwhile, a simplified CFD-DEM model that is considered to be suitable for dilute gas-solid two-phase simulation has been applied by Teng *et al.* [5] in Fluid Energy Mill simulation.

Pneumatic conveying is a method of transportation of granular particles in a pipeline using a gas stream. It is widely used in industries because of its cleanness, flexibility of layout, low maintenance cost and a high level of automation. Depending on its different modes, it can be categorized as dense and dilute phase. Bends, which are one of the most commonly used facilities to change flow direction in pneumatic conveying, are known to be one of the key parameters affecting the gas-solid flow structures.

The aim of this work is to figure out what extent a larger time step can still result in accurate prediction, and the applicability of the simplified CFD-DEM model in dilute pneumatic conveying. First, a simplified CFD-DEM model will be introduced. Subsequently, the relationship between the stiffness and the time step will be discussed, and methods to determine the two parameters will be given. Finally, the results of the simulations of pneumatic conveying with bends will be compared to examine the applicability of the simplified CFD-DEM model. The last part of the work has been presented and discussed at the 27th IAHR Symposium on Hydraulic Machinery and Systems, Montreal, 2014, and other part is an improved and enhance version.

Received January 16 2015; accepted for publication April 15 2015: Paper number O15022S
Corresponding author: Jun Du, PhD. candidate, dujun@whu.edu.cn

This paper was presented at the 27th IAHR Symposium on Hydraulic Machinery and Systems, September 4, Montreal, Canada.

2. Mathematical Model

Compared with the traditional CFD-DEM model, only the mutual momentum exchanges between the gas and solid phase are taken into consideration in the simplified CFD-DEM model, and the effect of the volume fraction on the gas phase is neglected. In every time step, there is no need to calculate the volume fraction of the gas phase. The differences between the traditional and the simplified CFD-DEM model can be seen in the gas phase governing equations.

2.1 Gas phase governing equations

The equation for conservation of mass, or continuity equation, can be written as follows:

The traditional model: $$\frac{\partial}{\partial t}(\varepsilon_g \rho_g) + \nabla \cdot (\varepsilon_g \rho_g \boldsymbol{u}_g) = 0 \tag{1}$$

The simplified model: $$\frac{\partial \rho_g}{\partial t} + \nabla \cdot (\rho_g \boldsymbol{u}_g) = 0 \tag{2}$$

The equation for conservation of momentum can be expressed as follows:

The traditional model: $$\frac{\partial}{\partial t}(\varepsilon_g \rho_g \boldsymbol{u}_g) + \nabla \cdot (\varepsilon_g \rho_g \boldsymbol{u}_g \boldsymbol{u}_g) = -\varepsilon_g \nabla p + \nabla \cdot (\varepsilon_g \boldsymbol{\tau}_g) + \varepsilon_g \rho_g \boldsymbol{g} - \boldsymbol{S} \tag{3}$$

The simplified model: $$\frac{\partial}{\partial t}(\rho_g \boldsymbol{u}_g) + \nabla \cdot (\rho_g \boldsymbol{u}_g \boldsymbol{u}_g) = -\nabla p + \nabla \cdot (\boldsymbol{\tau}_g) + \rho_g \boldsymbol{g} - \boldsymbol{S} \tag{4}$$

The coupling between the two phases is then achieved through the calculation of the momentum sink of the drag force that arises due to the relatively velocity between the phases. Therefore, the momentum sink $\boldsymbol{S}$ is calculated by

$$\boldsymbol{S} = \frac{1}{\Delta V} \sum_{i=1}^{i=n} \boldsymbol{f}_{p=g,i} \tag{5}$$

The gas-particle interaction force can be calculated by

$$\boldsymbol{f}_{p-g,i} = \boldsymbol{f}_B + \boldsymbol{f}_{drag,i} \tag{6}$$

2.2 Solid phase governing equations

According to DEM, a particle in a system can have two types of motion: translational and rotational, determined by Newton's second law of motion. The forces acting on a particle include gravity, contact force, drag force and other force, such as the van der Waales force and the capillary force. For simplicity, they are not considered in this work. Therefore, the governing equations for particle *i*, at any time, *t*, can be expressed as follows:

$$m_i \frac{d\boldsymbol{v}_i}{dt} = m_i \boldsymbol{g} + \boldsymbol{f}_{p-g,i} + \sum\nolimits_{j=1}^{k_i} (\boldsymbol{f}_{contact,ij} + \boldsymbol{f}_{damp,ij}) \tag{7}$$

and

$$\boldsymbol{I}_i \frac{d\boldsymbol{\omega}_i}{dt} = \sum\nolimits_{j=1}^{k_i} \boldsymbol{T}_{ij} \tag{8}$$

The equations used to calculate the forces and torques considered in this work have been listed in Table 1, and the coupling scheme is the same as that used in our previous study [10]. As such, it is not given in this paper.

Table 1 The formulation of forces and torques acting in governing equations[a].

Forces and torques	Formulation
The normal contact force, $\boldsymbol{f}^n_{contact,ij}$ [N]	$(4/3)E^* R^{*1/2} \delta_n^{3/2}$
The normal damping force, $\boldsymbol{f}^n_{damp,ij}$ [N]	$-2(5/6)^{1/2} \beta (S_n m^*)^{1/2} \boldsymbol{v}_n^{rel}$
The tangential contact force, $\boldsymbol{f}^t_{contact,ij}$ [N]	$S_t \delta_t$
The tangential damping force, $\boldsymbol{f}^t_{damp,ij}$ [N]	$-2(5/6)^{1/2} \beta (S_t m^*)^{1/2} \boldsymbol{v}_t^{rel}$
The torque, $\boldsymbol{T}_i$ [Nm]	$-\mu_t \boldsymbol{f}_n R_i \omega_i$
The drag force, $\boldsymbol{f}_{drag}$ [N]	$0.5 C_D \rho_g A \lvert \boldsymbol{v}_{p-g}^{rel} \rvert \boldsymbol{v}_{p-g}^{rel}$

[a] Where $1/E^* = (1-\nu_i^2)/E_i + (1-\nu_j^2)/E_j$, $1/R^* = 1/R_i + 1/R_j$, $1/m^* = 1/m_i + 1/m_j$, $\beta = \ln e / (\ln^2 e + \pi^2)^{1/2}$, $S_n = 2E^* (R^* \delta_n)^{1/2}$, $S_t = 8G^* (R^* \delta_n)^{1/2}$, $1/G^* = (2-\nu_i)/G_i + (2-\nu_j)/G_j$, $A = \pi R_i^2$, $Re = \varepsilon_g \rho_g D_p \lvert \boldsymbol{v}_{p-g}^{rel} \rvert / \mu_g$, $G_i = E_i / 2(1+\nu_i)$,

$$C_D = \begin{cases} 24/Re & Re \le 0.5 \\ 24(1.0 + 0.15 Re^{0.687})/Re & 0.5 \le Re \le 1000 \\ 0.44 & Re > 1000 \end{cases}.$$

3. Stiffness and time step

3.1 Background

Time step is considered as an important parameter in CFD-DEM. A larger time step can reduce the compute load, while it should be small enough to maintain a stable numerical solution. Previous studies indicate that a larger time step can be used by making particles less stiff or softer in based on DEM simulation [4,6-11]. Different time steps with various values of stiffness or Young's modulus have been used to simulate different gas-solid flow systems, as shown in Table 2. Determination of time step with different stiffness or Young's modulus in CFD-DEM is still an open problem.

Table 2 the values of Young's modulus or stiffness and time step used in previous CFD-DEM simulations

References	Young's Modulus, E [Pa]	Stiffness, k_n [N/m]	time step [s]
Tsuji *et al.* [1]	3×10^{9}	-	2×10^{-5}
Tsuji *et al.* [6]	-	800	2.11×10^{-4}
Xu and Yu [12]	-	5×10^{4}	1.5×10^{-5}
Feng and Yu [13]	1×10^{8}	-	2.5×10^{-6}
Zhou *et al.* [14]	1×10^{7}	-	1.75×10^{-7}

In principle, time steps for gas and particle phase should be same. However, in some computations, the time step for gas phase can be larger than that for particle phase because the effect from a single DEM iteration is too small to result in a considerable change in the gas phase, and the treatment can improve computational efficiency [5, 15, 16]. In practice, the first step to determine the time step in CFD-DEM is determination of that in DEM.

The principle that the time step is a fraction of the characteristic natural frequency has been widely accepted in CFD-DEM simulation [1, 4, 6, 17]. It seems that a larger time step can be selected if the particle stiffness is lower. Tsuji *et al.* [6] reported that calculation based on a smaller stiffness than an actual one did not show a large difference in particle motion from the calculation based on the actual stiffness in the cases, where the most dominant force causing particle motion was that of fluid. Di Renzo and Di Maio [18] considered that by reducing the elastic constant, the contact time and the time step were increased. Therefore, in order to select a suitable larger time step in dilute CFD-DEM simulation, there are two stages: choose an acceptable stiffness used in CFD-DEM, and determine a reasonable time step in CFD-DEM.

3.2 Choice of stiffness

Some investigators report the effect of the different stiffness on the particle behavior in various conditions including DEM and CFD-DEM simulations. Yuu *et al.* [7] simulated the motion of particles discharging from a rectangular hopper, whose stiffness were 7.0×10^{7}, 7.0×10^{5} and 7.0×10^{3} N/m. All of the calculated results not only qualitatively described the experimental results, but also approximately described the quantitative characteristics of the measured data. Rhodes *et al.* [9] found that bubbling and other fluidization bed characteristics in the simulations using stiffness of 800, 8000 and 80,000 N/m were all very similar. Moreno-Atanasio *et al.* [19] found that the contact stiffness did not influence appreciably the fluidization behavior for the low value of surface energy, but strongly influenced the behavior of the systems with the large value of surface energy. Lommen *et al.* [11] investigated and quantified the effects of particle stiffness on bulk material behavior. This research had shown that a reduction in particle stiffness could lead to undesirable effects, and suggested that users should be cautious and verified their approach when applying a particle reduction in models related to the bulk material behavior. Alobaid *et al.* [16] investigated the influences of the stiffness with small, moderate and high orders of magnitude on the simulation accuracy in dense fluidized bed. The results indicated that moderate stiffness showed a very good compromise between acceptable computing time and accuracy. Thus it can be seen that the effect of lower stiffness on particle behavior is still an issue of debate.

The normal overlap between the particles results from the momentum and stiffness of contacts. Lommen et al. [11] proposed that users should compare the normal overlaps, when they wanted to determine a feasible amount of stiffness reduction. Di Renzo and Di Maio [18] discussed the choice of the parameter values in the linear model and remarked that care must be taken when assigning arbitrary values, otherwise excessive overlaps were likely to occur. Malone and Xu [4] mainly investigated the contact parameters used in the linear-spring-dashpot model, and presented a simple method for determining a suitable value of stiffness for use in DEM simulations, based on an acceptable value of interparticle overlap. Alobaid *et al.* [16] calculated penetration depths from various stiffness coefficients with different diameters and relative velocities in linear modulus, and commented that the underestimation of the stiffness coefficients produced not only unphysical penetrations but also leaded to shrinkage of the entire bed volume in stationary case. In the following work, we concern about the relationship between the stiffness and the normal overlap in the non-linear Hertzian model.

In the non-linear Hertzian model, the normal stiffness is calculated by

$$k_n = \frac{4}{3} E^* \sqrt{R^*} \tag{9}$$

The equivalent Young's modulus and radius, respectively, are given by

$$\frac{1}{E^*} = \frac{1-\nu_i^2}{E_i} + \frac{1-\nu_j^2}{E_j} \tag{10}$$

$$\frac{1}{R^*} = \frac{1}{R_i} + \frac{1}{R_j} \tag{11}$$

In software EDEM, Young's Modulus is given by

$$E_i = 2(1+\nu_i)G_i \tag{12}$$

Therefore, the relationship between the normal stiffness and the normal overlap can be reflected by the relationship between the shear modulus and the normal overlap in the following.

In the numerical tests, a particle with an assuming impact velocity impacts a flat wall without the influence of gravity, and they have the same shear modulus. The normal overlaps with different values of shear modulus are examined. The orders of shear modulus vary from 10^3 Pa to 10^9 Pa. The lower limit is the stiffness value popular used in CFD-DEM simulations and the upper one is the order of polypropylene and polystyrene which are the popular materials used in gas-solid experiments. Other parameters used in these tests are shown in Table 3.

Table 3 Parameters used in the simulation test

Parameter	value
particle diameter, R_i [mm]	4
particle density, ρ[kg/m^3]	1123
coefficient of rolling friction, μ_r [-]	0.005
coefficient of static friction, μ_s [-]	0.3
coefficient of restitution, e [-]	0.4
Poisson ratio, ν_i [-]	0.3
time step [s]	1×10^{-8}

In Fig. 1, the percentage of the max normal overlap to the particle diameter is plotted against the shear modulus. It can be observed that the overlap increases with the decrease of the shear modulus. Take the impact velocity is 1 m/s as an example, when the value of shear modulus is greater than 5×10^6 Pa, the overlap keeps at a low magnitude which is less than 2%. The increase of the overlap begins to be evident when shear modulus continues to reduce. When shear modulus is 1×10^4 Pa, the percentage of the max normal overlap to the particle diameter approached to 25%. In the numerical tests, when the value of the shear modulus was set to less than 10^4 Pa, the particle goes through the impact flat and hence there is no overlap data. This value is 5×10^4 Pa and 1×10^5 Pa, respectively, when the impact velocity is 4m/s and 7 m/s. The result indicates that the magnitude of stiffness reduction will determine the level of overlap. As the level of overlap that is acceptable will be application-dependent, the value of shear modulus should be chosen according to their simulation condition. For a conservative principle in mind, 1×10^7 Pa which is two orders of magnitude smaller than the actual physical value, is considered as an acceptable shear modulus in the following sections.

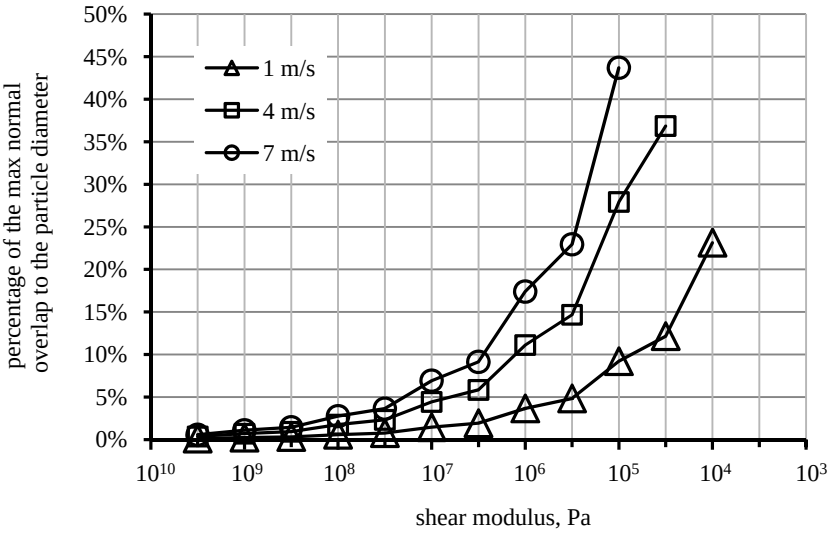

Fig. 1 The relationship between shear modulus and percentage of the max normal overlap to the particle diameter

3.2 Choice of stiffness

Malone and Xu [4] used a single particle test to determine a suitable time step with the linear-spring-dashpot model, and the energy conservation was studied in a perfectly elastic system. In the system, a particle drops from a given height, and the return height is noted to calculate the percentage relative error in energy conservation with a specified time step, which is a fraction of the natural frequency of the harmonic oscillation. As a matter of fact, the error in energy conservation occurs during the collision, and is directly reflected by the error of particle velocity. Therefore, the percentage relative error in energy conservation can be calculated by the particle velocity, and it saves more simulation time than that according to the return height. Moreover, Di Renzo and Di Maio [18] reported the collision time depended on the impact velocity, and the collision time is considered to be closely related to the choice of time step in DEM. Trial test also indicates that the percentage relative error in energy conservation is related to the collision velocity. Therefore, it is important to identify the initial height in above test. But Malone and Xu (2008) did not note how to identify that. However, the initial height has to be risen with the increase of collision velocity. It will make more

time be wasted in the part of no energy conservation error occurs. In order to save the test time, we improve a new method to test the error in energy conservation.

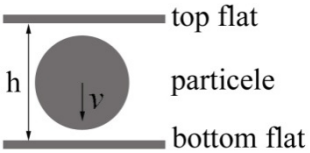

Fig. 2 Schematic representation of the perfectly elastic test system

In our method, the test is studied in a perfectly elastic system without the effect of gravity, and the particle velocity is noted to calculate the percentage relative error in energy conservation. The test system includes two flats, and the initial position of the particle locates in the middle of the flats as shown in Fig. 2. As gravity is not considered, the particle velocity remains unchanged once the collision contact finishes. After series of collisions, a group of velocities at the initial position is obtained. The percentage relative error in energy conservation is identified as follow:

$$(\frac{\max(|\boldsymbol{v}_i - \boldsymbol{v}_0|)}{v_0}) \times 100\% \tag{13}$$

Several time steps which are tested are given by:

$$\Delta t = C\sqrt{m_i / k_n} \tag{14}$$

where C is the fraction. The trial test indicates that the error velocity presents periodic fluctuation, and the periodicity approaches 400 times collision. Hence, these tests capture the results for a period of 500 times collision. In these tests, the initial velocity is set to 7 m/s, and the coefficient of restitution is equal to 1. The distance between top and bottom flat, *h*, is 5 mm which is a little larger than the particle diameter to save the test time, and other parameters are the same with Table 3.

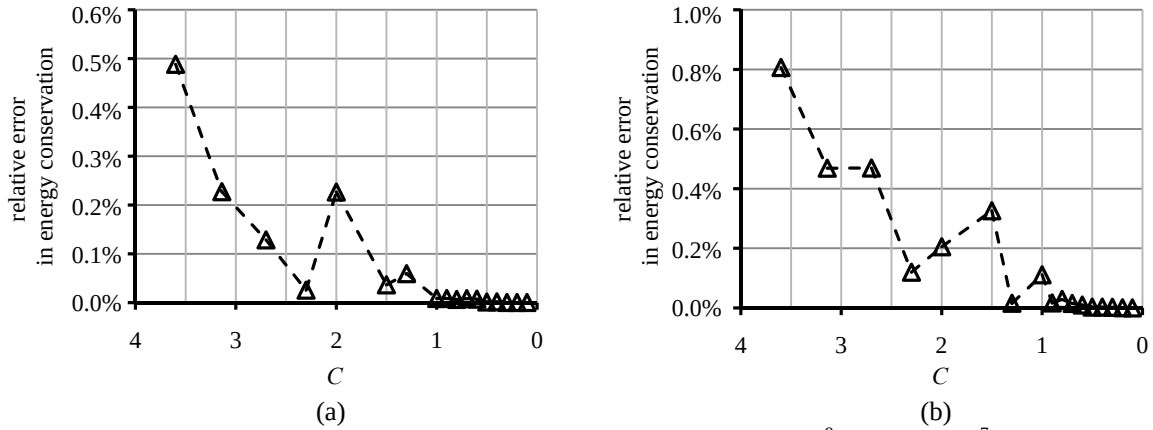

Fig. 3 Percentage relative error in energy conservation: (a) G=10^9 Pa; (b) G=10^7 Pa.

The percentage relative error in energy conservation as shown in Fig. 3, the relative error appears fluctuations, and the peak value decays with the decrease of the fraction. In this paper, we consider that if the fraction and less than that makes the relative error in energy conservation be less than 0.05%, the fraction is acceptable. According to this principle, the fractions are acceptable for 1×10^9 Pa and 1×10^7 Pa are 1and 0.9, respectively, and the corresponding time steps are 6.65×10^{-7} s and 5.98×10^{-6} s.

4. Simulation condition

In this work, there are three types of pipe systems simulated: the horizontal-vertical case, the vertical-horizontal case and the horizontal-horizontal case. The geometry of each case consists of three parts: the pipe with the inlet, the 90° bend section and the pipe with the outlet. The length of pipe with the inlet and the outlet are 0.5 m and 1 m, respectively. The sketches of the calculation domain of three cases are given in Fig. 4. The diameter of the pipe *D*=0.05 m and the bend radius ratio *R/D*=1.0. The shear modulus in this work is set to 1×10^7 Pa, and the time step should be less than 5.98×10^{-6} s. For convenience, the time step is set to 5×10^{-6} s. The parameters used in three cases are shown in table 4 and table 5.

Table 4 The same parameters used in three cases.

Phase	Parameter	Value
Solid	Density, ρ [kg/m^3]	1123
	Poisson ratio, v_i [-]	0.3
	Shear modulus, G [Pa]	1×10^7
	Coefficient of restitution,e [-]	0.4
	Coefficient of static friction, μ_s [-]	0.3
	Coefficient of rolling friction, μ_r [-]	0.005
	Time step [s]	5×10^{-6}
	Particle velocity at inlet, $\boldsymbol{v}_i$ [m/s]	7

Gas	Density, ρ_g [kg/m^3]	1.225
	Viscosity,μ_g [kg/m·s]	1.8×10^{-5}
	Time step [s]	5×10^{-4}

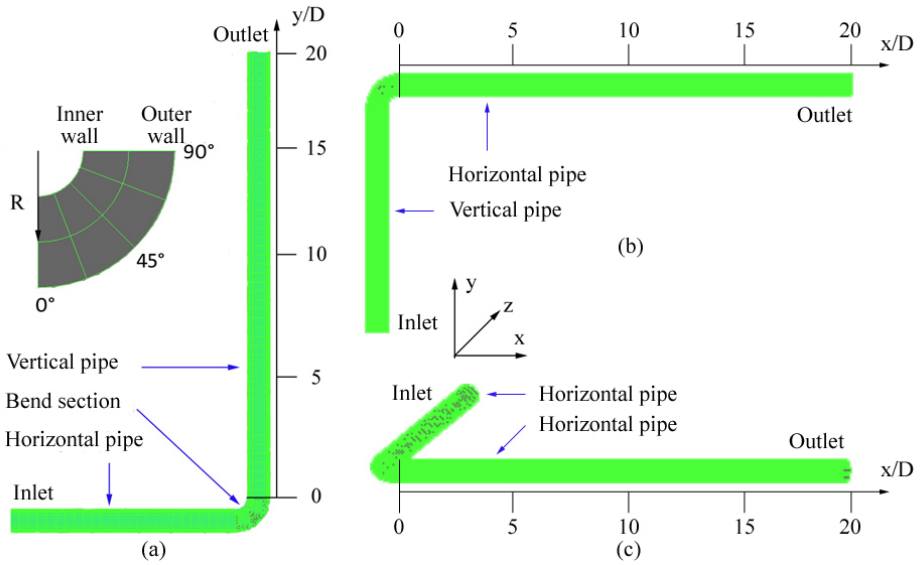

Fig. 4 Schematic representation of the simulation: (a) the horizontal-vertical case; (b) the vertical-horizontal case; (c) the horizontal-horizontal case.

Table 5 The different parameters used in three cases.

Phase	Parameter	Value		
		the horizontal-vertical case	the vertical-horizontal case	the horizontal-horizontal case
Solid	Mass flow rate, G_s [kg/m^{2}s]	31.1	40.8	35.7
	Particle radius, R_i [mm]	1.4	1.5	1.5
Gas	Velocity, $\boldsymbol{u}_g$ [m/s]	11.9	16	16

5. Results and discussion

A particle rope which carries most of conveyed materials in a small portion of the pipe cross-section is considered as the most typical characteristic of gas-solid flow in a bend. The key features of gas-solid flow in a bend include the particle rope formation and dispersion, and particle velocity reduction, and can be captured by both CFD-DEM models. Fig. 5 shows the solid flow structure and the particle velocity in pneumatic conveying system with different types of bends from the simplified CFD-DEM model. The features of the rope dispersion in different types of bends seem different. In the horizontal-vertical case, the rope disperses after the particles move out of the bend and distribute uniform in the downstream of the vertical pipe. In the vertical-horizontal pipe, as the effect of the gravity, the rope disperses quickly and the particles settle at the bottom of the horizontal pipe. In the horizontal-horizontal case, The particle rope does not disperse directly along the direction of the gravity. The particles move along a spiral line and keep close to the inside of the pipe when they exit from the bend section. They finally settled at the bottom of the pipe and move to downstream. In the following, the rope dispersion rate and the particle velocity in the cross-sections will be compared to verify the applicability of the simplified CFD-DEM model in dilute pneumatic conveying simulation.

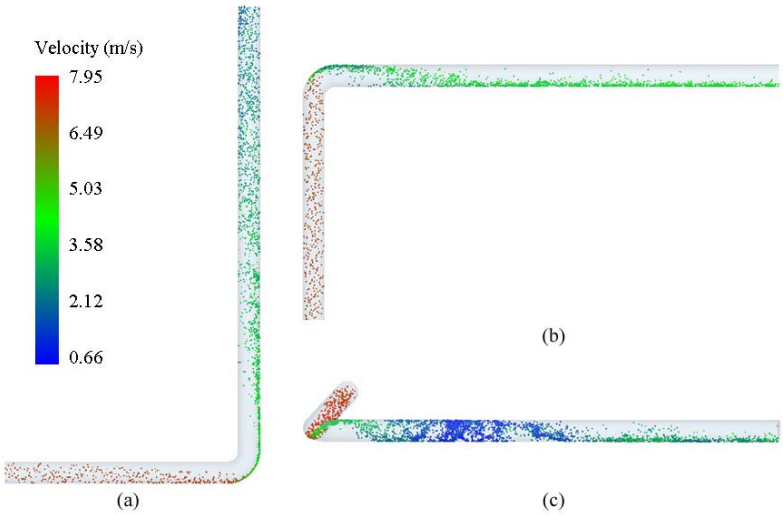

Fig. 5 The solid flow structure and the particle velocity of horizontal-vertical case at t=2 s: (a) the simplified model; (b) the traditional model.

Fig. 6 compares the particle concentration and velocity profiles at the cross-section in the vertical pipe of the horizontal-vertical case for simplified and traditional CFD-DEM models. The particle distribution percentage from the inner wall (x/D=0.0) to the outer wall (x/D=1.0) at different locations can represent the particle concentration in the pipe. At y/D=3, the particles concentrate near the outer wall, and the concentrations began to decrease at y/D=5, as shown in Figure 6(a). It is clearly that the results from both CFD-DEM models are remarkably consistent. The particle velocity profile at y/D=10 is given in Figure 6(b). the particle velocity near the outer wall seems consistent from two models and some differences near the inner wall, but the differences are limited.

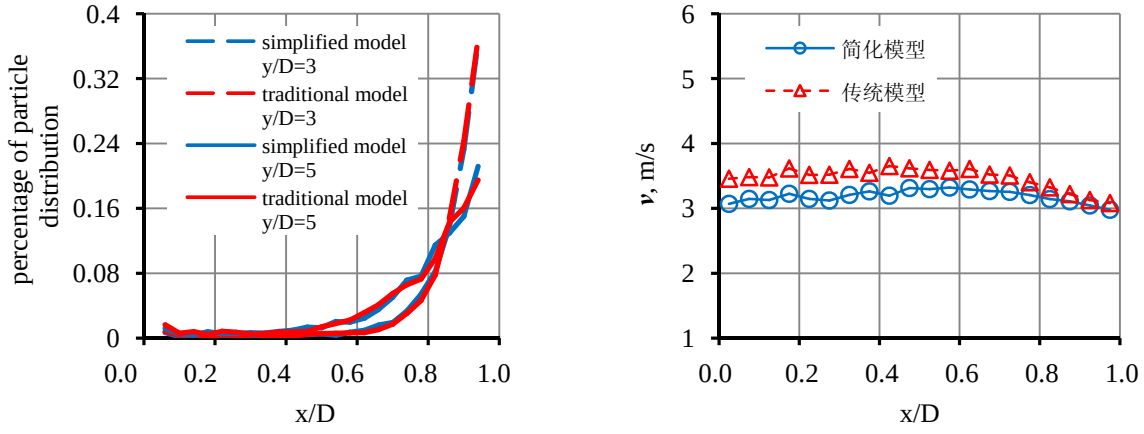

Fig. 6 The particle concentration and velocity profile at the cross-section in the vertical pipe: (a) percentage of particle distribution; (b) particle velocity at y/D=10.

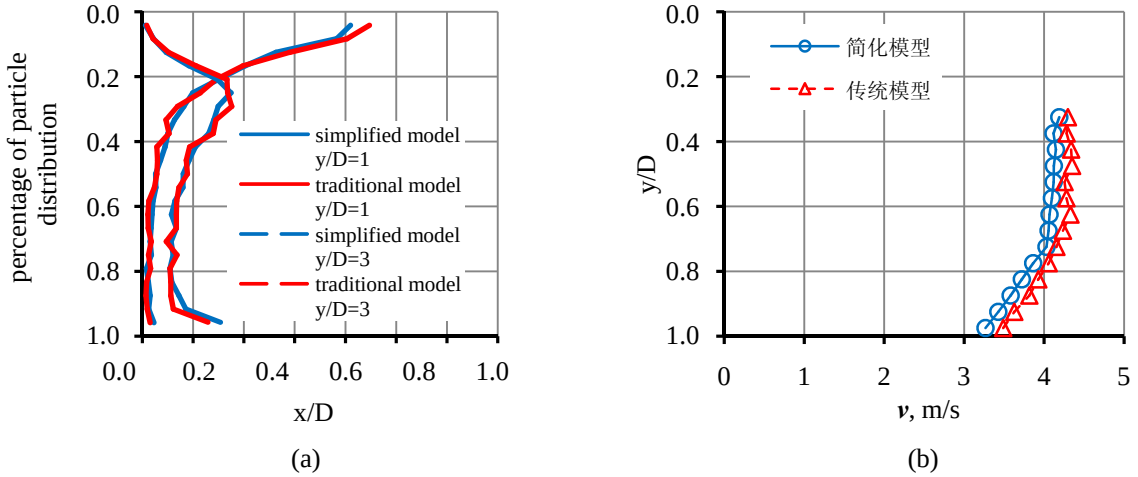

Fig. 7 The particle concentration and velocity profile at the cross-section in the horizontal pipe: (a) percentage of particle distribution; (b) particle velocity x/D=10.

The particle concentration and velocity profiles of the vertical-horizontal case are shown in Fig. 7. At x/D=1, the particles concentrate near the top of the pipe and move to the bottom of the pipe quickly. At x/D=3, the peak of the particle distribution has been located between the axial and the top wall. The predictions for simplified and traditional CFD-DEM are also consistent, as shown in Figure 7(a). The particle velocity profile at x/D=10 shows that the velocity near the bottom of the pipe is less than that near the axial, and the result from the simplified model seems a little slow.

Fig. 8 shows the particle distribution at different cross-sections in horizontal pipe. At exit of the bend (x/D=0), the particle rope is strong, and the particles distribute in a small area, the predictions for two models seem same. At x/D=7, most of the particles can distribute close to the inside of the pipe wall, but some of particles have been fallen down from the top of the pipe. At x/D=9, more particles disperse in the pipe, and there are less particles at the top of the pipe. It indicates that the particle rope has began to disperse at x/D=7. It is clear that the result for the simplified model predict a faster rope dispersion in horizontal-horizontal case.

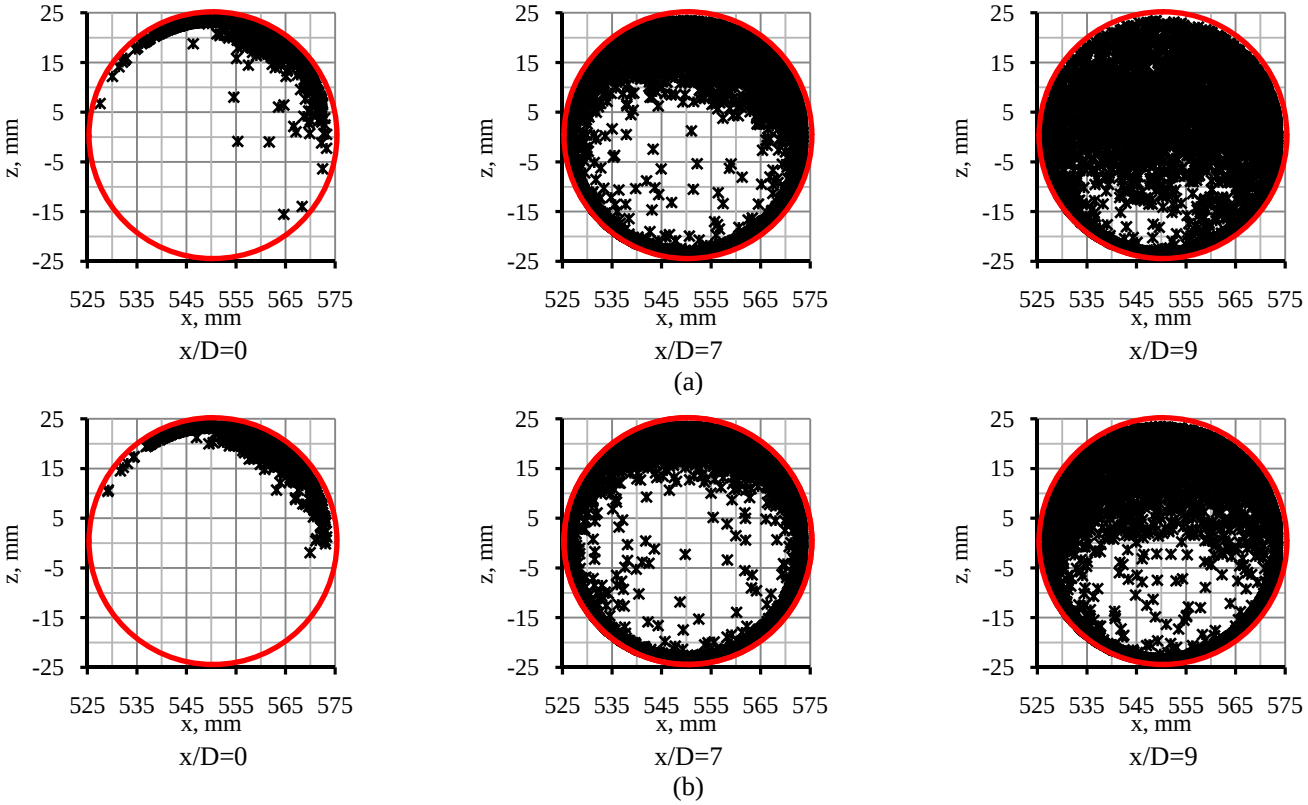

Fig. 8 particle distribution at different cross-sections in horizontal pipe from t=1 s to t=3 s: (a) the simplified model; (b) the traditional model.

Fig. 9 compares the particle velocity at different cross-sections in horizontal-horizontal case for the simplified model and the traditional model. The simplified model predicts a lower particle velocity at the exit of bend than the traditional model. The velocity is minimum at x/D=6 for the simplified model and at x/D=7 for the traditional model.

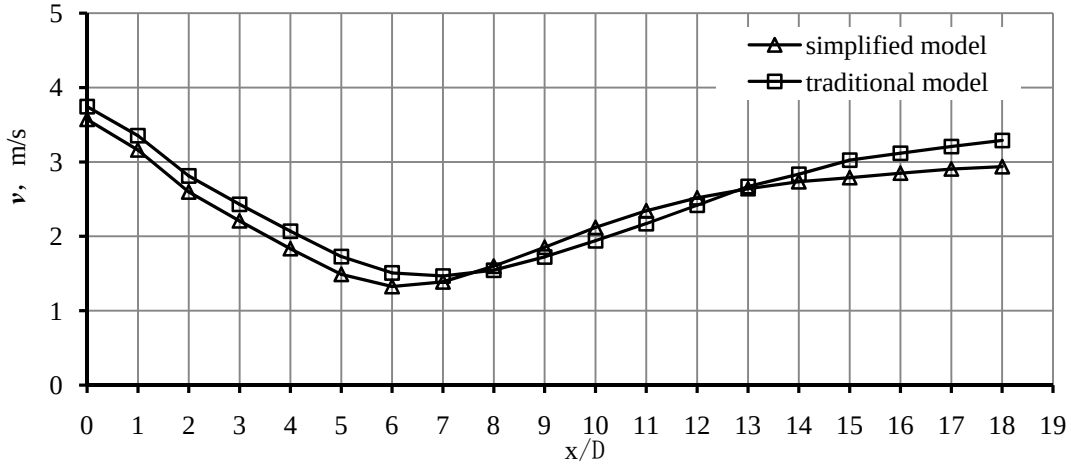

Fig. 9 the particle velocity at different cross-sections in horizontal-horizontal case

6. Conclusion

This research supplies two methods to accelerate CFD-DEM simulation: a larger time step and a simplified CFD-DEM model. The numerical tests indicate that two orders of magnitude smaller stiffness just cause a little increase of overlap in non-linear Hertzian model. The time step can be determined by testing the percentage relative error in energy conservation, and a larger one can be selected by reduction of the stiffness. The simplified CFD-DEM model that ignores the effect of the solid fraction on the gas phase governing equations is less compute-intensive and keeps the simulation stable. Its applicability on dilute phase has been examined by compared the prediction of pneumatic conveying with bends for traditional CFD-DEM model. Both of the models can obtain the same particle rope features in different types of bends. For the rope dispersion rate and the particle velocity, the simplified model obtains a similar results with traditional model in horizontal-vertical case and vertical-horizontal case, and has a significant difference in horizontal-horizontal case.

Acknowledgments

Acknowledgments may be made to individuals or institutions who have made an important contribution

Nomenclature

$\boldsymbol{u}_g$	Gas velocity [m/s]	Re	Reynolds number [-]
$\boldsymbol{g}$	Gravity force vector [N/kg]	C_D	Drag coefficient [-]
$\boldsymbol{S}$	Moment sink [N/m^3]	δ	Particle overlap [m]
$\boldsymbol{f}_{p\text{-}g,i}$	Particle-gas interaction force [N]	ε_g	Volume fraction [-]
$\boldsymbol{f}_B$	Buoyance force [N]	D_p	Particle diameter [m]
m_i	Particle mass [kg]		
$\boldsymbol{I}_i$	Particle moment of inertia [Kg•m^2]		**Greek Symbols**
$\boldsymbol{v}_i$	Particle translational velocity [m/s]	$_n$	Normal component
$\boldsymbol{\omega}_i$	Particle rotational velocity [s^{-1}]	$_t$	Tangential component
G	Shear modulus [Pa]	i,j	Particle number

References

[1] Tsuji Y., Tanaka T., Ishida T., 1992, “Lagrangian numerical simulation of plug flow of cohesionless particles in a horizontal pipe,” Powder Technology, Vol. 71, No. 3, pp. 239-250.

[2] Zhu H.P., Zhou Z.Y., Yang R.Y., 2007, “Discrete particle simulation of particulate systems: Theoretical developments,” Chemical Engineering Science, Vol. 62, No. 13, pp. 3378-3396.

[3] Zhu H.P., Zhou Z.Y., Yang R.Y., 2008, “Discrete particle simulation of particulate systems: A review of major applications and findings,” Chemical Engineering Science, Vol. 63, No. 23, pp. 5728-5770.

[4] Malone K.F., Xu B.H., 2008, “Determination of contact parameters for discrete element method simulations of granular systems,” Particuology, Vol. 6, No. 6, pp. 521-528.

[5] Teng S.L., Wang P., Zhang Q., 2011, “Analysis of Fluid Energy Mill by gas-solid two-phase flow simulation,” Powder Technology, Vol. 208, No. 3, pp. 684-693.

[6] Tsuji Y., Kawaguchi T., Tanaka T., 1993, “Discrete particle simulation of two-dimensional fluidized bed,” Powder Technology, Vol. 77, No. 1, pp. 79-87.

[7] Yuu S., Abe T., Saitoh T., 1994, “Three-dimensional numerical simulation of the motion of particles discharging from a rectangular hopper using distinct element method and comparison with experimental data (effects of time steps and material properties),” Advanced Powder Technology, Vol. 6, No. 4, pp. 259-269.

[8] Kawaguchi T., Tanaka T., Tsuji Y., 1998, “Numerical simulation of two-dimensional fluidized beds using the discrete element method (comparison between the two- and three-dimensional models),” Powder Technology, Vol. 96, No. 2, pp. 129-138.

[9] Rhodes M.J., Wang X.S., Nguyen M., 2001, “Use of discrete element method simulation in studying fluidization characteristics: influence of interparticle force,” Chemical Engineering Science, Vol. 56, No. 1, pp. 69-76.

[10] Brosh T., Kalman H., Levy A., 2014, “Accelerating CFD-DEM simulation of processes with wide particle size distributions,” Particuology, Vol. 12, pp. 113-121.

[11] Lommen S., Schott D., Lodewijiks G., 2014, “DEM speedup: Stiffness effects on behavior of bulk material,” Particuology, Vol. 12, pp. 107-112.

[12] Xu B.H., Yu A.B., 1997, “Numerical simulation of the gas-solid flow in a fluidized bed by combining discrete particle method with computational fluid dynamics,” Chemical Engineering Science, Vol. 52, No. 16, pp. 2785-2809.

[13] Feng Y.Q., Yu A.B., 2004, “Assessment of model formulations in the discrete particle simulation of gas-solid flow,” Industrial & Engineering Chemistry Research, Vol. 43, No. 26, pp. 8278-8290.

[14] Zhou Z.Y., Kuang S.B., Chu K.Y., 2007, “Discrete particle simulation of particle-fluid flow: model formulations and their applicability,” Journal of Fluid Mechanics, Vol. 661, pp. 482-510.

[15] Chu K.W., Yu A.B., 2008, “Numerical simulation of the gas-solid flow in three-dimensional pneumatic conveying bends,” Industrial & Engineering Chemistry Research, Vol. 47, No. 18, pp. 7058--7071.

[16] Alobaid F., Baraki N., Epple B., 2014, “Investigation into improving the efficiency and accuracy of CFD/DEM simulations,” Particuology, Vol. 16, pp. 41-53.

[17] Mishra B.K., Murty C.V.R., 2001, “On the determination of contact parameters for realistic DEM simulations of ball mills,”

Powder Technology, Vol. 115, No. 3, pp. 290-297.
[18] Di Renzo A., Di Maio F.P.D., 2004, “Comparison of contact-force models for the simulation of collisions in DEM-based granular flow codes,” Chemical Engineering Science, Vol. 59, No. 3, pp. 525-541.
[19] Moreno-Atanasio R., Xu B.H., Ghadiri M., 2007, “Computer simulation of the effect of contact stiffness and adhesion on the fluidization behaviour of powders,” Chemical Engineering Science, Vol. 62, No. 1-2, pp. 184-194.